Transaction A: Civil Engineering
Vol. 16, No. 4, pp. 331–339

SCIENTIA IRANICA

Numerical Investigation of the Effects of Soil Densification on the Reduction of Liquefaction-Induced Settlement of Shallow Foundations

H. Shahir[1] and A. Pak[1,*]

Abstract. *The liquefaction phenomenon is usually accompanied by a large amount of settlement. Based on the observations made in past earthquakes, ground improvement by densification is one of the most useful approaches to reduce the liquefaction-induced settlement. Currently, there is no analytical solution for evaluation of the amount of settlement and tilting of footings that are constructed on densified ground surrounded by liquefiable soil. A number of factors, such as underlying soil properties, dimensions of the footing and earthquake loading characteristics, cause the problem to become complicated. In this paper, the dynamic response of shallow foundations on both liquefiable and non-liquefiable (densified) soils is studied using a 3D fully-coupled dynamic analysis. A well-calibrated critical state two-surface plasticity model has been used in the numerical analysis, which is capable of accounting for the volumetric/shear response of the soil skeleton at a wide range of densities (void ratios) and confining pressures. The OpenSEES platform is used to conduct the numerical simulations. The proposed numerical model has been applied in simulating a series of centrifuge experiments. Comparison of the numerical results and the centrifuge experiment measurements reveals that the numerical model is capable of capturing the important aspects of the dynamic response of footings on liquefiable and densified subsoils, and can be used as a valuable tool for investigating the amount of liquefaction-induced settlement, tilting of footings and their reduction due to densification.*

Keywords: *Liquefaction; Ground improvement; Densification; Shallow foundation; Settlement.*

INTRODUCTION

The settlement and tilting of buildings due to liquefaction are major causes of structural damage during earthquakes. One of the main approaches to reduce liquefaction damage is ground improvement by densification-based methods such as vibro-floatation, dynamic compaction and blasting. The effectiveness of densification in mitigating the effects of liquefaction can be demonstrated by reviewing the low level of damage in shallow foundations built on densified zones during major seismic events as far back as the 1964 Niigata earthquake [1,2]. Observations in field case histories indicate that by densification throughout the full liquefiable soil thickness and adequate lateral extent, the displacement of the foundation decreases considerably in comparison to the adjacent unimproved areas. The observations, however, reveal that some deformation may be expected, even when the total liquefiable depth is improved especially at high intensity of shaking.

Current design practice, regarding the use of densification as a liquefaction resistance measure, is mostly based on the mitigation of liquefaction triggering by a reasonable safety margin. In this design procedure, the amount of reduction of the foundation settlement under earthquake loading is unknown. Currently, there is no standard design procedure for evaluating the amount of foundation settlement considering soil improvement measures employed to mitigate liquefaction.

1. *Department of Civil Engineering, Sharif University of Technology, Tehran, P.O. Box 11155-9313, Iran.*
*. *Corresponding author. E-mail: pak@sharif.edu.*

Received 9 July 2008; received in revised form 12 January 2009; accepted 2 March 2009

The seismic response of a shallow foundation on a saturated granular soil layer subjected to seismically-induced liquefaction is complicated. The evaluation of liquefaction-induced settlement and tilting requires modeling the process of liquefaction and subsequent consolidation and its effect on the behavior of shallow foundations. Quantitative analysis of liquefaction can only be accomplished by considering the coupled interaction of the soil skeleton and the pore fluid. For this purpose, a suitable formulation for the behavior of the two-phase continuum and a proper constitutive model are required.

In some numerical investigations, the influence of soil liquefaction on the soil-structure interaction phenomenon has been studied [3-6]. These modelings generally consist of simulation of the dynamic interaction between a homogeneous liquefying soil layer and a structure resting on the ground surface, using a 2D (plane strain assumption) coupled finite element analysis. To the best of the authors' knowledge, the dynamic response of a shallow foundation on improved ground by compaction methods has not yet been investigated. There are, however, a number of centrifuge experiments, in which the reduction of a foundation settlement due to subsoil densification has been studied [2,7,8]. The experimental measurements indicate that, as the compaction depth increases, the settlement and tilting of footing decreases. It was observed that there is a definite depth, below which, further compaction has a minor effect on reducing the foundation settlement. Liu and Dobry [7] determined this depth to be equal to 1.5 times the footing width, which was equivalent to 0.55 times of the total liquefiable soil thickness. Hausler [2] obtained this depth equal to 1.75 times of the footing width, which was 0.7 times of the total liquefiable soil thickness. The centrifuge experiments performed by Coelho et al. [8] revealed that the most important benefit, resulting from the enlargement of the width of the improved region, is the reduction of the post-earthquake settlement of the foundation.

In this paper, a 3D finite element model, composed of a fully coupled dynamic analysis and a well-calibrated constitutive model, is introduced in simulating the seismic response of shallow foundations on saturated granular soil strata. OpenSEES [9] has been used to conduct the numerical simulations. OpenSEES is an open-source software framework developed at PEER (Pacific Earthquake Engineering Research Center) for simulating the seismic response of structural and geotechnical systems. A series of centrifuge experiments is simulated to show the model capability in capturing the important aspects of the dynamic response of footings on liquefiable and densified subsoils.

FULLY COUPLED DYNAMIC ANALYSIS OF SATURATED POROUS MEDIA

For a fully coupled analysis, equilibrium or momentum balance for the soil-fluid mixture, momentum balance for the fluid phase and, finally, the mass balance for the whole system of soil and fluid must be satisfied. The unknowns in this complete set of equations are displacements of the solid phase (u_s), displacements of the fluid phase relative to the solid phase (u_{rf}) and pressure of the fluid phase (P). It is convenient to reduce the number of variables by neglecting the terms that have little influence on the results. For dynamic problems in which high-frequency oscillations are not important, such as earthquake loading, the relative velocity of the fluid phase has little effect on the system and can be disregarded [10]. Therefore, the governing equations are reduced to two. The primary variables in this form of equation are solid displacements and fluid pressure. Thus, this form is called $u_s - P$ or for simplicity $u - P$ formulation.

Using the finite element method for spatial discretization, the $u - P$ formulation is as follows:

$$M\ddot{U} + \int_v B^T \sigma' dV - QP - f^{(s)} = 0, \tag{1a}$$

$$Q^T \dot{U} + HP + S\dot{P} - f^{(p)} = 0, \tag{1b}$$

where M is the mass matrix, U is the solid displacement vector, B is the strain-displacement matrix, σ' is the effective stress tensor, Q indicates the discrete gradient operator coupling the motion and flow equations, P is the pore pressure vector, S is the compressibility matrix, and H is the permeability matrix. Vectors $f^{(s)}$ and $f^{(p)}$ include the effects of body forces, external loads and fluid fluxes. Details of the above mentioned matrices and vectors can be found in Zienkiewics and Shiomi [10].

THE CRITICAL STATE TWO-SURFACE PLASTICITY SAND MODEL

A plasticity constitutive model developed by Dafalias and Manzari [11] was employed for modeling of the monotonic and cyclic behavior of sand. The formulation of the model is based on the two-surface plasticity theory [12], within the critical state soil mechanics framework [13].

A schematic representation of the two-surface model in the π-plane is shown in Figure 1. In this model, the isotropic hypoelasticity assumption is adopted with the elastic moduli as a function of current pressure and void ratio. The yield surface is a circular cone with its apex located at the origin. The size of the yield surface is normally considered a constant

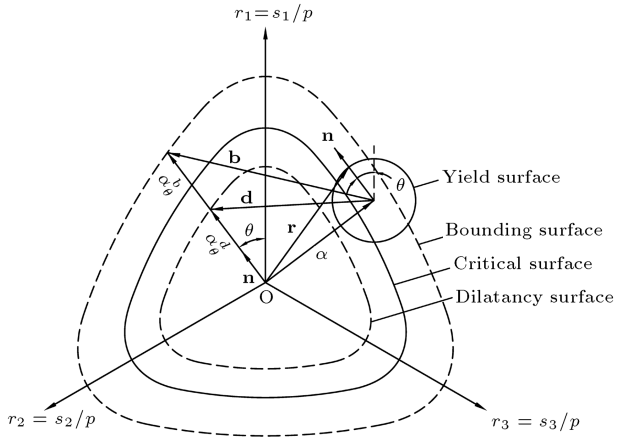

Figure 1. Schematic representation of the two-surface model in the π-plane [11].

(no isotropic hardening) of rather small value in most applications. This model includes three other surfaces, namely bounding (peak), dilatancy and critical. The critical surface is in direct correspondence to the critical stress ratio in the triaxial space. The critical state of a soil [13] is attained when the stress ratio, $\eta = q/p$, equals the critical stress ratio, (M), which is a material constant. In the current model, the bounding and dilatancy stress ratios are related to the critical stress ratio by way of the "state parameter" as follows:

$$M^b = M \exp(-n^b \psi), \qquad M^d = M \exp(n^d \psi), \qquad (2)$$

where M^b and M^d are peak and dilatancy stress ratios and n^b and n^d are positive material constants. $\psi = e - e_c$ is the "state parameter" proposed by Been and Jefferies [14], where e is the current void ratio of the soil element and e_c is the critical void ratio corresponding to the existing confining stress. The following power relationship is used to define the Critical State Line (CSL):

$$e_c = e_0 - \lambda_c \left(\frac{p_c}{p_{at}}\right)^{\xi}, \qquad (3)$$

where e_0, λ_c and ξ are critical state constants.

As shown in Figure 1, the bounding and dilatancy surfaces are shown by dash lines, indicating their change with ψ, and the critical surface by a solid line. All surfaces are fully determined by the value of state parameter ψ and this increases the numerical efficiency of the model. Also, the state parameter includes the combined effect of density (void ratio) and confining stress. Thus, one of the main features of the current constitutive model is its applicability to all densities and confining pressures with one set of material constants.

The plastic modulus (K_p) and dilatancy coefficient (D) are related to the distance from the bounding and dilatancy surfaces as follows:

$$K_p = \frac{2}{3} p h \mathbf{b} : \mathbf{n}, \qquad (4)$$

$$D = A_d \mathbf{d} : \mathbf{n}. \qquad (5)$$

The vectors **b** and **d** shown in Figure 1, are defined as the vectors connecting the current stress state to its image on the bounding and dilatancy surfaces, respectively; p is the mean effective stress and h is a positive scalar-valued function. A_d is a function including the effects of "fabric change phenomenon" arisen during stress increment reversal after a dilative plastic volumetric strain occurrence.

The "distance dependent plastic modulus" is the main feature of the classical bounding surface model [12]. In the current model, the dilatancy coefficient is also defined based on the basic idea of "distance dependency" in the bounding surface model.

The constants of the Dafalias and Manzari model were calibrated for Toyoura sand [11]. However, in this research, the centrifuge experiments that were chosen for numerical simulation have been conducted using Nevada sand. Therefore, the model constants were calibrated for Nevada sand using the triaxial test data performed under different conditions [15]. A list of the model constants is shown in Table 1. The model has 15 constants divided into 6 categories based on their functions.

VARIABLE PERMEABILITY FUNCTION

The shaking of a saturated sand deposit results in the structural change of the soil skeleton and a decrease

Table 1. Material parameters of the critical state two-surface plasticity model for Nevada sand.

Constant	Variable	Value
Elasticity	G_0	150
	ν	0.05
Critical state	M	1.14
	c	0.78
	λ_c	0.027
	e_0	0.83
	ξ	0.45
Yield surface	m	0.02
Plastic modulus	h_0	9.7
	c_h	1.02
	n^b	2.56
Dilatancy	A_0	0.81
	n^d	1.05
Fabric-dilatancy tensor	$z_{\max}$	5
	c_z	800

in the void ratio. Due to the void ratio reduction, the permeability coefficient of the sand must decrease. However, this reduction in void ratio and its effect on permeability is not significant. On the other hand, structural changes in the soil skeleton results in a reduction of the pore shape factor and tortuosity, which cause a significant increase in the permeability coefficient during liquefaction [16]. At the onset of liquefaction, soil particles lose full contact with each other which creates easier paths for water to flow. The creation of such flow paths reduces pore shape factor and tortuosity and, consequently, leads to an increase in the permeability coefficient at the time of initial liquefaction. The basic mechanism that is involved in this phenomenon is the pore pressure increase.

Based on the research performed by Shahir et al. [15], there is a direct relationship between the permeability coefficient and the excess pore pressure ratio for all pore pressure build-up, liquefaction, and dissipation phases. They proposed the following function for the variations of permeability coefficient in simulation of the liquefaction process:

$$\frac{k}{k_i} = \begin{cases} 1+(\alpha-1)\times r_u^{\beta_1} & \text{in build-up phase } (r_u<1.0) \\ \alpha & \text{in liquefied state } (r_u = 1.0) \\ 1+(\alpha-1)\times r_u^{\beta_2} & \text{in dissipation phase } (r_u<1.0) \end{cases} \quad (6)$$

where k is the soil permeability coefficient during the process of liquefaction, k_i is the initial (at-rest) permeability coefficient before shaking and α, β_1 and β_2 are positive material constants. r_u is the excess pore pressure ratio, defined as follows:

$$r_u = \Delta u/\sigma'_{v0}, \quad (7)$$

where Δu is the excess pore water pressure and σ'_{v0} is the initial vertical effective stress.

The above formulation was implemented into OpenSEES for updating the coefficient of permeability at the end of each time step during seismic analysis. For this purpose, a new element with a formulation similar to the element of EightNodeBrick_u_p from the UCD (University of California, Davis) computational geomechanics toolset [17], was created with addition of the variable permeability function.

Then, it was applied to simulate the behavior of a saturated sand layer subjected to earthquake loading in the centrifuge experiment. By comparing the numerical results with centrifuge experimental observations, the constants were calibrated as follows:

$$\alpha = 20, \qquad \beta_1 = 1.0, \qquad \beta_2 = 8.9.$$

This basically means that the permeability coefficient increases up to 20 times during the initial liquefaction. The amount of increase in permeability coefficient during liquefaction was reported in some investigations. Arulanandan and Sybico [16], based on the measurement of changes in the electrical resistance of saturated sand deposits in the centrifuge tests, concluded that the "in-flight permeability" of saturated sand during liquefaction increases up to 6 to 7 times greater than its initial value. Jafarzadeh and Yanagisawa [18], by measurement of the volume of expelled water from saturated sand columns in shaking table model tests, indicated that the average permeability coefficient during excitation is 5 to 6 times greater than its static value. This is nearly equivalent to an increase of 10 to 12 times in the peak value of permeability during liquefaction. In this study, the choice of this increasing factor (α) is essentially to obtain the best fit with the centrifuge results, which have been obtained 2 to 3 times greater than the reported values from experimental evidence. From a practical viewpoint, this difference can be attributed to the inaccuracy involved in the measurement of the initial permeability coefficient.

Incorporation of the permeability variation in the numerical model is necessary for capturing both pore pressure and settlement responses of a liquefiable soil mass. Therefore, the above mentioned variable permeability function has been used in numerical simulations conducted in this research.

VERIFICATION OF THE NUMERICAL MODEL BY CENTRIFUGE EXPERIMENTS

Description of the Centrifuge Experiment

For verification of the numerical model, the centrifuge experiments conducted by Hausler [2] were considered. Hausler [2] carried out several centrifuge experiments to study the effects of ground improvement on the response of shallow footings under different conditions. Four centrifuge experiments were selected here for numerical modeling in which the effects of improvement depth on the foundation settlement and other responses are studied.

The centrifuge model 1 consisted of a square rigid structure rested on approximately 20 meters of liquefiable Nevada sand with an initial relative density (D_r) of 30%, which was placed in a flexible container. A sketch of the geometry of the experiments is presented in Figure 2. In models 2 to 4, the soil beneath the structure was compacted up to a relative density of 85% with different depths of 6 m (0.3 H improved), 14 m (0.7 H improved) and 20 m (full depth improved). The initial relative density of the surrounding unimproved soil was 30%. The improved zone was square in plan and symmetric around the foundation axis, and the width of the improvement zone was approximately

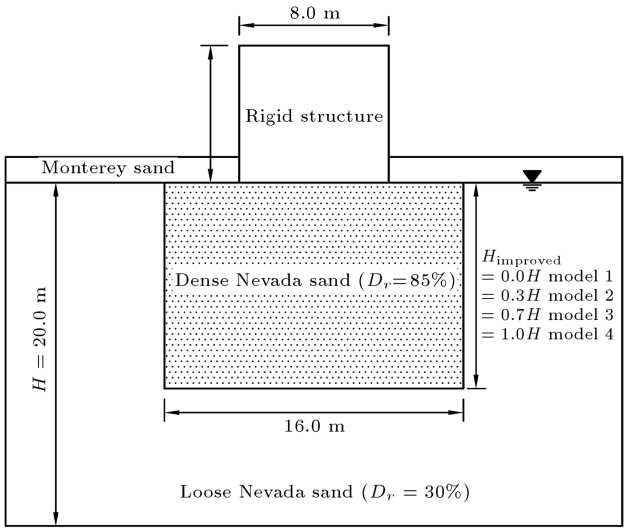

Figure 2. Geometry of the centrifuge experiments [2].

twice the foundation width. The structure is a cubic rigid block with the same dimension of 8 meters in all directions and a bearing pressure of 96 kPa embedded 1.0 m in the top dry soil.

The pore fluid used in the experiments had a viscosity 10 times greater than that of water and the model was spun up to a centrifuge acceleration of 40 g. Considering the scaling laws in centrifuge modeling [19], this experiment simulates a soil deposit with a permeability coefficient 4 times greater than that of Nevada sand in a prototype scale.

All models were shaken with a sequence of three scaled (small, large and medium) versions of the 83 m depth, N-S component of the 1995 Kobe Port Island earthquake. In this paper, only the small scale event with a peak ground acceleration of 0.15 g, which was applied prior to other shakings, was analyzed. The prototype time history of the input motion is shown in Figure 3.

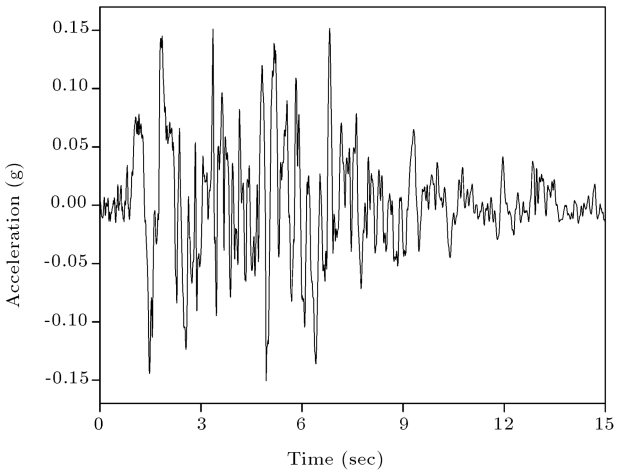

Figure 3. Prototype time history of the input motion.

Description of the Numerical Model

Numerical modeling of the centrifuge experiments was performed in a prototype scale. A three-dimensional finite element mesh with 1960 8-node cubic elements was used in the analyses, as shown in Figure 4. Table 2 lists the properties of Nevada sand used in the analyses. To consider the effect of a laminar box in the numerical simulation, the lateral boundaries perpendicular to the direction of shaking were constrained together to have the same displacement in the direction of shaking. The displacements of lateral boundaries parallel to the direction of shaking were tied in the direction perpendicular to shaking. The bottom boundary was assumed fixed. Full dissipation of the pore pressure was allowed through the surface of the sand layer and the lateral and bottom boundaries were supposed to be impervious. The structure was modeled by rigid brick elements connected rigidly to the adjacent soil nodes. The Young's modulus for the structure is chosen large enough (2×10^7 kPa) so that the structure can be considered rigid.

Analyses were carried out in three steps. First, a static analysis was performed to apply the gravitational forces due to the self weight of the soil and, also, the weight of the structure. After this step, the resultant displacement, velocity and acceleration vectors were zeroed, and the initial effective stresses and pore water pressures were stored. Then, the earthquake loading was applied as a prescribed acceleration time history at the bottom boundary. During seismic analysis, the variation of permeability coefficient was incorporated in the analysis using Equation 6. After the ending of earthquake loading, the consolidation phase, to allow redistribution and dissipation of the developed excess pore pressures, was analyzed.

The above mentioned three steps of analysis were performed for each of the 4 models, i.e. 0.0, 0.3 H, 0.7 H, and 1.0 H soil improvement depths.

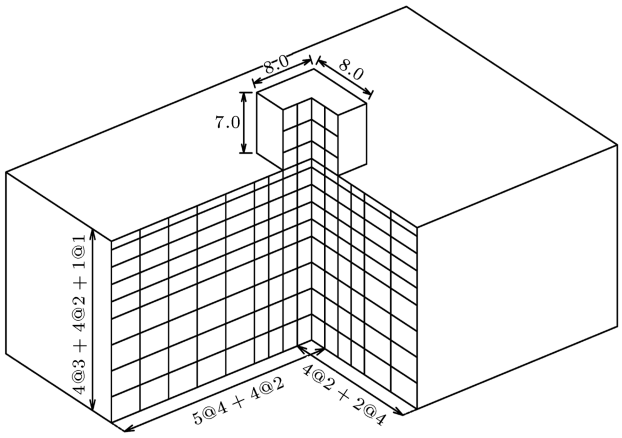

Figure 4. Cross section of the 3D finite element mesh (all dimensions are in m).

Table 2. Properties of Nevada sand used in the analyses [2].

Parameter	Value at $D_r = 30\%$	Value at $D_r = 85\%$
Void ratio	0.781	0.586
Saturated unit weight	19.0 kN/m^3	20.15 kN/m^3
Water permeability	4.0×10^{-5} m/sec	2.5×10^{-5} m/sec
Prototype permeability	1.6×10^{-4} m/sec	1.0×10^{-4} m/sec

RESULTS AND DISCUSSION

Excess Pore Pressure

Figures 5 and 6 display the predicted and measured maximum excess pore pressure ratios along the soil depth under the foundation centerline and at free field, respectively. It is noted that the maximum excess pore pressure ratios at all elevations do not occur at the same time. The maximum excess pore pressure ratios were presented in tabular format by Hausler [2] and the digital data of the centrifuge experiments was not available. Thus, the time history of excess pore pressures could not be compared and the maximum excess pore pressure ratios were used for comparison.

As shown in Figure 6, the occurrence of liquefaction ($r_u = 1.0$) up to the depth of about 12.0 m in the free field was accurately predicted by the numerical model. The zero depth represents foundation bottom level. In deeper strata, both numerical simulation and the experimental model indicate that the condition of zero effective stress or initial liquefaction state did not occur. The predicted pore pressure ratios in the free field from all four models are nearly the same and match well with the measured values. At the bottom of the soil layer, the predicted pore pressure ratio is somewhat greater than the measured one (Figure 6).

The predicted excess pore pressure ratios presented in Figure 5 are generally in good agreement

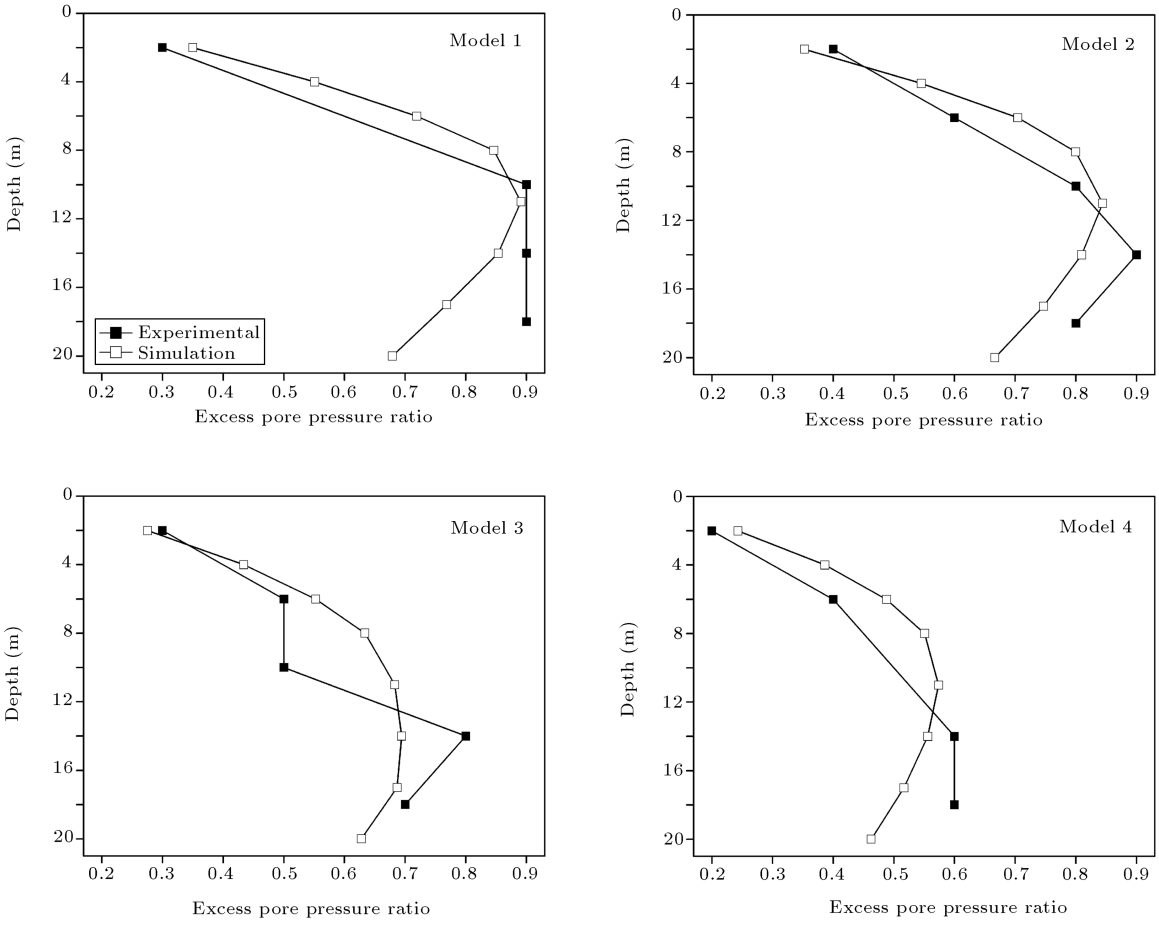

Figure 5. Distribution of excess pore pressure ratio along the soil depth under the foundation.

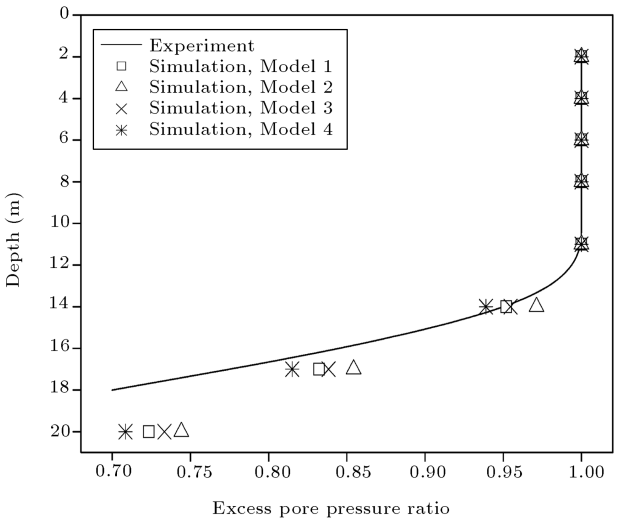

Figure 6. Distribution of excess pore pressure ratio along the soil depth at free field.

with the experimental measurements. According to the experimental measurements, as well as simulation results, densification had a major influence on reduction of the developed excess pore pressure ratio beneath the foundation. The average excess pore pressure ratios under the foundation in Model 4 are about 65% of Model 1. It is noted that, even in Model 1, in which no ground improvement was made and where the developed excess pore pressure under the foundation was higher than other improved models, the initial liquefaction state was not observed beneath the foundation. Contrary to the observed behavior in the free field, the experimental and numerical results in all four models show that the minimum excess pore pressure ratio occurs at shallow depths beneath the foundation and increases gradually downward. The maximum excess pore pressure ratio, however, does not occur at the bottom of the models but rather at some intermediate depth.

The difference between the pattern of excess pore pressure ratio in the free field and beneath the foundation is mainly attributed to differences between the initial vertical effective stresses. The initial vertical effective stress used for calculating the excess pore pressure ratio (Equation 7) is due to the effective weight of the soil layers in the free field. However, under the foundation, the effect of the foundation load also contributes to excess pore pressure. Therefore, the values of excess pore pressure ratios under the foundation are substantially lower than those in the free field.

Structure Settlement and Tilting

The measured and predicted foundation settlements versus normalized compaction depth in all experiments are presented in Figure 7a. Figure 7b shows the foundation settlement normalized to the free field soil settlement. The measured free field settlement in the experiments varies between 20 to 25 cm and the predicted value for the free field settlement is about 20 cm in all numerical models. In Figure 7b, the influence of different free field settlements has been removed by normalization of the foundation settlement. As seen in this figure, the predicted settlements are in good agreement with the experimental observations.

The normalized foundation settlement has decreased from 2.13 in the experiment without compaction to 0.43 in the experiment with full depth compaction, i.e. the foundation settlement has decreased about 5 times due to densification. This indicates the effectiveness of densification in mitigation of the liquefaction induced settlement. As observed in Figure 7, there is a rather negligible reduction of foundation

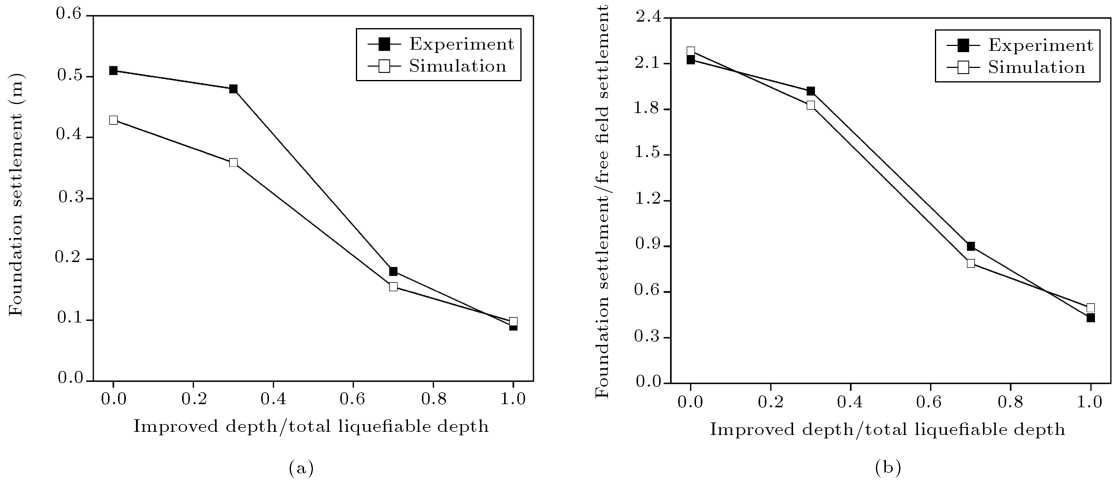

Figure 7. Foundation settlement versus normalized compaction depth. (a) Absolute amounts of settlement; (b) Normalized values.

settlement in the case of superficial compaction up to a depth of 0.3 H (H: total soil depth). The major reduction in foundation settlement is achieved when the improved zone extends through 0.7 H. Further compaction below the depth of 0.7 H has a minor effect on reducing the amount of foundation settlement. It is noted that the obtained values may not be generalized for other situations and more research is warranted, considering a wide range of soils, foundations and shaking parameters.

In Figure 8, distribution of the foundation settlement along the soil depth is shown. The measured values, by installation of the settlement pads, are only available for Experiments 1 and 4, which are presented in this figure. As shown, the predicted and measured values show good similarities. In the cases of uniform subsoil under the foundation (Experiments 1 and 4), the results indicate that the lowest vertical strains occurred at shallow and deep layers (about 0-4 and 16-20 m). This confirms the previous finding that superficial compaction as well as further deep compaction has minor influence on reducing the foundation settlement. In partially compacted experiments, the major part of settlement occurs in the loose layer. As shown in Figure 8, in Experiment 3, 55% of the foundation settlement is due to the vertical strain of the loose layer where its thickness is only 30% of the total depth.

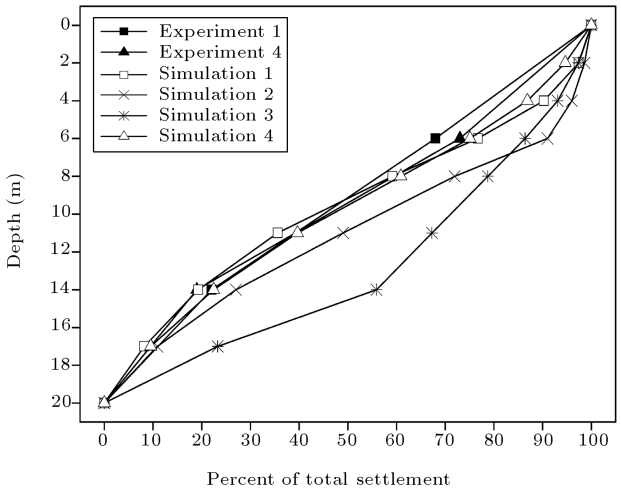

Figure 8. Distribution of foundation settlement along soil depth.

Another important quantitative assessment regarding the performance of the improved ground is the tilting of the structure (differential settlement divided by structure width). Figure 9a displays the predicted time history of the structure tilting in all of the experiments. In Figure 9b, the predicted maximum transient and permanent tilting of the structure is compared with the experimental measurements. The predicted and measured values differ significantly. However, both experimental and simulation results indicate that although the influence of superficial compaction on total settlement reduction is minor, it reduces the structure tilting considerably. Therefore, if the total settlement is not a concern, a superficial compaction may suffice for elimination of the differential settlement. The general implication of this result, however, requires extensive experimental and numerical investigation.

SUMMARY AND CONCLUSION

In this study, a 3D fully coupled dynamic analysis was applied for simulating the seismic response of shallow foundations on both liquefiable and non-liquefiable (densified) subsoils in a series of centrifuge experiments. By employing the critical state two-surface plasticity model and taking the variability of permeability into account, it becomes possible to obtain good results for pore pressure variation in the

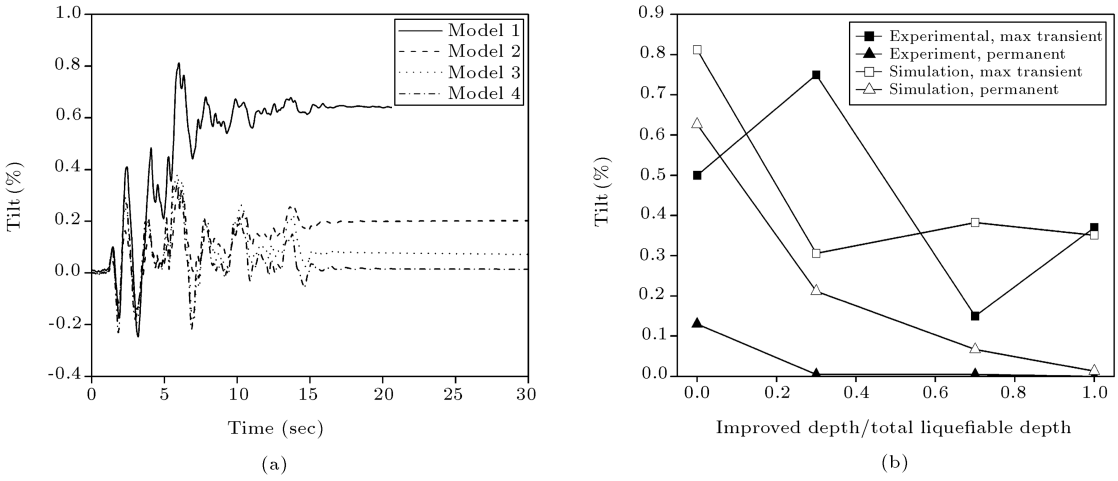

Figure 9. (a) Predicted time history of structure tilting; (b) Maximum transient and permanent tilting of structure versus normalized compaction depth.

soil mass beneath a shallow foundation and, also, to predict reliable values for foundation settlement.

The simulation results indicate that the values of excess pore pressure ratio under the foundation are substantially less than those in the free field, owing to the effects of the structure surcharge, and so, contrary to the free field, the liquefaction state is not observed beneath the foundation. Soil densification proved to have a major effect on reducing the developed excess pore pressure ratio beneath the foundation.

The effectiveness of densification in the reduction of the liquefaction-induced settlement has been simulated well. The simulation results, as well as experimental measurements, reveal that further compaction below the depth of 0.7 H has a minor effect on reducing the amount of foundation settlement. It was shown that, although superficial compaction has a minor influence on reducing settlement, it is able to reduce the structure tilting considerably.

REFERENCES

1. Mitchell, J.K., Baxter, C.D.P. and Munson, T.C. "Performance of improved ground during earthquakes", *Proceeding of Soil Improvements for Earthquake Hazard Mitigation*, Geotechnical Special Publication No. 49, ASCE, pp. 1-36 (1995).
2. Hausler, E.A. "Influence of ground improvement on settlement and liquefaction: A study based on field case history evidence and dynamic geotechnical centrifuge tests", PhD Dissertation, University of California, Berkeley (2002).
3. Koutsourelakis, S., Prevost, J.H. and Deodatis, G. "Risk assessment of an interacting structure-soil system due to liquefaction", *Earthquake Engineering and Structures Dynamics*, **31**(4), pp. 851-79 (2002).
4. Chakrabortty, P., Popescu, R. and Prevost, J.H. "Tower structures on liquefiable soil excited by random seismic input", *9th ASCE Specialty Conference on Probabilistic Mechanics and Structural Reliability*, Albuquerque (2004).
5. Popescu, R., Prevost, J.H., Deodatis, G. and Chakrabortty, P. "Dynamics of nonlinear porous media with applications to soil liquefaction", *Soil Dynamics and Earthquake Engineering*, **26**, pp. 648-65 (2006).
6. Lopez-Caballero, F. and Modaressi Farahmand-Razavi, A. "Numerical simulation of liquefaction effects on seismic SSI", *Soil Dynamics and Earthquake Engineering*, **28**, pp. 85-98 (2008).
7. Liu, L. and Dobry, R. "Seismic response of shallow foundation on liquefiable sand", *Journal of Geotechnical and Geoenvironmental Engineering, ASCE*, **123**(6), pp. 557-567 (1997).
8. Coelho, P.A.L.F., Haigh, S.K., Madabhushi, S.P.G. and O'brein, T.S. "Post-earthquake behavior of footings employing densification to mitigate liquefaction", *Ground Improvement*, **11**(1), pp. 45-53 (2007).
9. *OpenSees (Open System for Earthquake Engineering Simulation) Platform*, Developed by the Pacific Earthquake Engineering Research Center (PEER), at the University of California, Berkeley, http://opensees.berkeley.edu/.
10. Zienkiewics, O.C. and Shiomi, T. "Dynamic behavior of saturated porous media: The generalized Biot formulation and its numerical solution", *International Journal for Numerical Methods in Engineering*, **8**, pp. 71-96 (1984).
11. Dafalias, Y.F. and Manzari, M.T. "Simple plasticity sand model accounting for fabric change effects", *Journal of Engineering Mechanics*, **130**(6), pp. 622-634 (2004).
12. Dafalias, Y.F. "Bounding surface plasticity, I: Mathematical foundation and hypoplasticity", *Journal of Engineering Mechanics*, **112**(9), pp. 966-987 (1986).
13. Schofield, A.N. and Wroth, C.P., *Critical State Soil Mechanics*, McGraw-Hill, New York (1968).
14. Been, K. and Jefferies, M.G. "A state parameter for sands", *Geotechnique*, **35**(2), pp. 99-112 (1985).
15. Shahir, H., Pak, A. and Taiebat, M. and Jeremic, B. "Evaluation of variation of permeability in liquefiable soil under earthquake loading", *Submitted to Soil Dynamics and Earthquake Engineering.*
16. Arulanandan, K. and Sybico, J. Jr. "Post-liquefaction settlement of sand", *Proceeding of the Wroth Memorial Symposium*, Oxford University, England (1992).
17. Jeremic, B. "Development of geotechnical capabilities in OpenSees", Pacific Earthquake Engineering Research Center, Report PEER 2001/12 (2001).
18. Jafarzadeh, F. and Yanagisawa, E. "Settlement of sand models under unidirectional shaking", *First International Conference on Earthquake Geotechnical Engineering*, K. Ishihara, Ed., IS-Tokyo, pp. 693-698 (1995).
19. Schofield, A.N. "Dynamic and earthquake centrifuge geotechnical modeling", *Proceeding of International Conference on Recent Advances in Geotechnical Earthquake Engineering and Soil Dynamics*, University of Missouri-Rolla, MO, pp. 1081-1100 (1981).